HHS Public Access

Author manuscript

Transl Res. Author manuscript; available in PMC 2024 July 01.

Published in final edited form as:

Transl Res. 2023 July ; 257: 43–53. doi:10.1016/j.trsl.2023.01.005.

Topical Captopril: A Promising Treatment for Secondary Lymphedema

Stav Brown, MD,

Gabriela D. García Nores, MD,

Ananta Sarker, BS,

Catherine Ly, MD,

Catherine C. Li, MD,

Hyeung Ju Park, PhD,

Geoffrey E. Hespe, MD,

Adana Campbell, MD,

Raghu P. Kataru, PhD,

Omer Aras, MD,

Babak J. Mehrara, MD

Plastic and Reconstructive Surgery Service, Department of Surgery, Memorial Sloan Kettering Cancer Center, 1275 York Ave, New York, New York 10065, USA

Abstract

Transforming growth factor-beta 1 (TGF-β1)-mediated tissue fibrosis is an important regulator of lymphatic dysfunction in secondary lymphedema. However, TGF-β1 targeting can cause toxicity and autoimmune complications, limiting clinical utility. Angiotensin II (Ang II) modulates intracellular TGF-β1 signaling, and inhibition of Ang II production using angiotensin-converting enzyme (ACE) inhibitors, such as captopril, has antifibrotic efficacy in some pathological settings. Therefore, we analyzed the expression of ACE and Ang II in clinical lymphedema biopsy specimens from patients with unilateral breast cancer-related lymphedema (BCRL) and mouse models, and found that cutaneous ACE expression is increased in lymphedematous tissues. Furthermore, topical captopril decreases fibrosis, activation of intracellular TGF-β1 signaling pathways, inflammation, and swelling in mouse models of lymphedema. Captopril treatment also improves lymphatic function and immune cell trafficking by increasing collecting lymphatic pumping. Our results show that the renin-angiotensin system in the skin plays an important role in the regulation of fibrosis in lymphedema, and inhibition of this signaling pathway may hold merit for treating lymphedema.

*Correspondence: Babak J. Mehrara, MD, 328 East 62nd Street, New York, New York 10065, Phone: (646) 803-8639, Fax: (212) 717-3677, mehrarab@mskcc.org.

Keywords

Lymphedema; fibrosis; inflammation; TGF-β1; lymphatic

Introduction

Secondary lymphedema is a common complication of cancer treatment, which affects an estimated 1 in 1000 Americans.[1] Patients with lymphedema have recurrent skin infections, pain, and decreased function.[2] Despite its prevalence, the treatment of lymphedema remains palliative, relying primarily on compression garments and physical therapy.[3] The lack of effective targeted treatments for lymphedema is largely related to a poor understanding of the pathophysiology of the disease.

Dermal fibrosis and fibrotic obliteration of lymphatic collectors are histological hallmarks of lymphedema. Clinical and experimental studies have shown that the degree of fibrosis positively correlates with the severity of lymphedema.[4–6] Transforming growth factor beta-1 (TGF-β1) is an important regulator of fibrosis in many pathological settings, including secondary lymphedema, and contributes to increased fibroblast collagen deposition, decreased extracellular matrix turnover, and modulated inflammatory responses.[6–10] Inhibition of TGF-β1 activity in mouse models of lymphedema decreases skin fibrosis and tissue swelling, and improves lymphatic function.[6, 9, 10] However, long-term TGF-β1 inhibition can cause toxicity and autoimmune complications limiting the clinical relevance of this approach.[11] Therefore, other approaches for inhibiting TGF-β1 activity and inhibiting fibrosis in lymphedema may be more promising.

The renin-angiotensin system (RAS) plays an important role in renal and cardiovascular physiology and also regulates fibrosis in various organ systems by modulating intracellular TGF-β1 signaling.[12–14] Angiotensinogen is synthesized in the liver and other tissues and is converted to angiotensin I (Ang I) by renin. Ang I, an inactive peptide, is converted to Ang II by angiotensin-converting enzyme (ACE) and exerts the physiologic effects of the RAS. ACE inhibitors or Ang II receptor antagonists effectively inhibit fibrosis by decreasing TGF-β1 activity and intracellular SMAD activation in cardiac, renal, and hepatic models of fibrosis.[15–24] A topical formulation of the ACE inhibitor captopril was also effective in decreasing skin fibrosis.[25]

Given these findings, we hypothesized that the RAS might also play a role in the pathophysiology of lymphedema. Thus in this study, we analyzed the RAS in clinical lymphedema skin biopsy specimens and investigated the potential of ACE inhibition in treating secondary lymphedema.

Material and Methods

Clinical lymphedema specimens

All procedures were approved by the Institutional Review Board (IRB) at Memorial Sloan Kettering Cancer Center (MSK) (IRB protocol 17-377). Inclusion criteria included: female, age 21-75 years, unilateral axillary surgery, and stage I–III lymphedema. Exclusion criteria

included pregnant or lactating, history of limb infection, chemotherapy or treatment with steroids/other immunosuppressive agents in the past 3 months, and recurrent breast cancer. Full-thickness skin biopsies (5 mm) were harvested from the volar surface of the normal and lymphedematous limbs at a point located 5–10 cm below the elbow crease. Surgery was performed under sterile conditions with local anesthesia. A single dose of antibiotics (cephalexin 1000 mg or clindamycin 600 mg if penicillin-allergic) was administered 30–60 min before the procedure. All patients provided written informed consent.

Mouse models of lymphedema

All experimental animal protocols were reviewed and approved by the Institutional Animal Care and Use Committee at MSK and were conducted per the National Institutes of Health (NIH) Guide for the Care and Use of Laboratory Animals, the Animal Welfare Act, and the Animal Scientific Procedures Act. Adult female wild-type (WT; C57BL/6J; #000664) mice aged 6-8 weeks were purchased from The Jackson Laboratory (Bar Harbor, Maine) and used for tail surgery and popliteal lymph node dissection (PLND). All mice were maintained in a pathogen-free, temperature- and light-controlled environment and fed ad libitum.

Isoflurane (Henry Schein Animal Health; Dublin, OH) was used for anesthesia, and the depth of anesthesia was checked at least every 15 min by monitoring tail reflex and respiratory rate. Mice were euthanized by carbon dioxide asphyxiation per protocols recommended by the Guidelines on Euthanasia by the American Veterinary Medical Association.

The tail model of lymphedema was performed using our previously published methods.[26, 27] Briefly, a 2-mm circumferential portion of the skin and superficial lymphatic vessels were excised 2 cm from the tail base, after which the deep collecting lymphatic vessels were ligated. Identification of these vessels is aided by the injection of Evans blue dye (Sigma-Aldrich; St. Louis, MO) into the distal tail before surgery.

The PLND model was also performed using our published methods.[26, 28] Briefly, an incision was made over the popliteal fossa, and the popliteal lymph node and surrounding fat (including the afferent and efferent lymphatics) were excised. The incision was closed with continuous 3-0 non-absorbable sutures.

Captopril treatment

Topical captopril was formulated with the Research Pharmacy Core Facility at MSK. Five percent captopril (Tokyo Chemical Industry; Tokyo, Japan) was dissolved in Aquaphor® (Beiersdorf; Hamburg, Germany) using 2.5% glycerin as a levigating agent. Aquaphor® with 2.5% glycerin without captopril was used as the control.

The initiation and duration of captopril treatment in the tail and PLND models were based on our previous studies.[29, 30] 4 mg of 5% captopril cream or vehicle control was applied circumferentially to the tail skin distal to the area where skin and lymphatics were excised. In the PLND model, we applied 2 mg of 5% captopril cream to the medial aspect of the hindlimb covering the area extending between the popliteal area and the foot. Topical treatment for both the tail model and animals treated with PLND was initiated 2 weeks

after surgery and performed once daily for 4 weeks (tail model) or 2 week (PLND model) thereafter. In the tail model, tissue analysis was performed 6 weeks after surgery based on previous reports indicating that the peak of pathology in terms of edema and fibrosis in this model is observed at that time point.[27, 31–36]

Tail volume measurements

Tail volume measurements were performed using our published method with the truncated cone formula $V = 1/4\pi\ (C_1C_2 + C_2C_3 + C_3C_4)$.[29] Tail diameters were measured in a standard fashion at 1 cm increments starting at the surgical site using a digital caliper (VWR; Radnor, Pennsylvania).

Western blot

Protein was isolated from clinical biopsy samples using the T-PER™ Tissue Protein Extraction Reagent (Thermo Scientific; Waltham, MA) and quantified using the Bradford method. Western blotting was performed using rabbit polyclonal anti-Ace1 (1:1000; #ab28311) from Abcam (Cambridge, MA), rabbit polyclonal anti-Ang II (1:250; #251229) from Abbiotec (Escondido, CA) and goat polyclonal anti-VEGF C (C-20) (1:100; #SC1881) from SantaCruz Biotechnology (Santa Cruz, CA). Loading controls included GAPDH (monoclonal anti-GAPDH; 1:1000; #MAB 374; Millipore Sigma; Burlington, MA) and β-actin (1:1000; #3700; Cell Signaling Technology, Inc.; Danvers, MA). Enhanced chemiluminescence (ECL) detection system was used to detect immunoreactivity. Image J software was used for quantification of band intensity. Relative expression analysis was performed using GraphPad Prism software version 9.3.

Histology and immunohistochemistry

Tail and hindlimb tissues were harvested 1 cm distal to the surgical site for histological and immunohistochemical analysis. Tissues were fixed in 4% paraformaldehyde (Sigma-Aldrich) at 4°C overnight, decalcified using 5% ethylenediaminetetraacetic acid (EDTA; Santa Cruz Biotechnology; Santa Cruz, CA), embedded in paraffin, and sectioned at 5 μm.

H&E staining was performed using a standard protocol with Mayer's hematoxylin (Lillie's Modification; Dako North America; Carpinteria, CA) and eosin Y solution (Thermo Fisher Scientific; Waltham, MA). After staining, the tissue sections were dehydrated with alcohol, extracted with xylene (Sigma-Aldrich), and then mounted with VectaMount Permanent Mounting Medium (Vector Laboratories, Inc.; Burlingame, CA).

For immunofluorescent staining, cut sections were rehydrated, and heat-mediated antigen unmasking was performed with sodium citrate (Sigma-Aldrich) in a 90°C water bath. Non-specific binding was blocked with 2% bovine serum albumin and 20% donkey serum in phosphate-buffered saline for one hour at room temperature. Tissues were incubated overnight with varying combinations of primary antibodies at 4°C. The primary antibodies used included rabbit monoclonal anti-ACE (1:100; #ab75762), rabbit polyclonal anti-Ang II (1:200; #251229) from Abbiotec, rabbit polyclonal anti-collagen I (1:100; #ab34710), rat monoclonal anti-F4/80 (1:100; #ab16911), and rabbit polyclonal anti-Ki67 (1:100; #ab15580) from Abcam (Cambridge, MA); rabbit polyclonal anti-CD3 (1:100; #A0452)

from Dako (Glostrup, Denmark); goat polyclonal anti-LYVE-1 (1:400; #2125), and goat polyclonal anti-podoplanin (1:100; #AF3244) from R&D Systems (Minneapolis, MN); mouse monoclonal anti-alpha smooth muscle actin (α-SMA) (1:100; #A2547) from Sigma-Aldrich and Rabbit monoclonal anti-Smad3 (#ab52903) from Abcam (Cambridge, MA). The following morning, the sections were washed and then incubated with corresponding fluorescent-labeled secondary antibody conjugates (1:1000; Life Technologies; Thermo Fisher) at room temperature for 5 hours, followed by 4,6-diamidino-2-phenylindole (DAPI; #D1306, Molecular Probes/Invitrogen; Eugene, OR) for 10 min for nuclear staining. Stained sections were mounted with Mowiol (Sigma-Aldrich).

Mounted sections were scanned with a Zeiss Mirax slide scanner (Munich, Germany) and analyzed with Pannoramic Viewer (3D Histech; Budapest, Hungary). Two blinded reviewers performed all analyses using a minimum of 3 high-powered fields per specimen. Type I collagen deposition and ACE expression were quantified as a percentage of the positively stained dermis and subcutaneous tissues within a fixed threshold to total tissue area using Metamorph Offline Software (Molecular Devices; Sunnyvale, CA).[37] Fibroadipose thickness was measured as the width of tissues bounded by the reticular dermis and deep fascia in four standardized regions of tail cross-sections. Cell counts and lymphatic vessel area were quantified in standardized areas measuring 0.25 mm^2. Cells were considered perilymphatic if they were measured within 50 μm of a lymphatic vessel. A comparison of α-SMA accumulation was performed by evaluating the points of greatest thickness in each cross-section.

Quantitative PCR (qPCR)

Total RNA was extracted using TRIzol (Invitrogen, Carlsbad, CA, USA) according to the manufacturer's instruction, and complementary DNA (cDNA) was prepared by using Maxima™ H Minus cDNA Synthesis Master Mix (Thermo Scientific; Rockford, IL). Quantitative PCR (qPCR; ViiA7; Life Technologies; Carlsbad, CA) was performed in duplicates using predesigned primer sets (Quantitect Primer Assays; Qiagen, Germantown, MD). Relative mRNA expression was analyzed and normalized to housekeeping genes, β-actin or GAPDH. Relative mRNA expression was log-transformed to adjust for distribution, and statistical analysis was performed using paired T-tests.

Near-infrared (NIR) lymphangiography

NIR lymphangiography was performed to evaluate lymphatic collecting vessel pumping function using a modification of previously published techniques.[38] Before the procedure, hair was removed from the hindlimbs using a depilatory cream to allow optimal lymphatic vessel visualization. Subsequently, 15 μl of 0.15 mg/ml indocyanine green (ICG; Sigma-Aldrich) was injected intradermally in the first webspace of the dorsal hindlimbs, after which mice were allowed to freely ambulate for 20 min to promote uptake of ICG into the lymphatic vasculature. Mice were then anesthetized and placed on a heating pad for imaging with a custom-made EVOS EMCCD camera (Life Technologies; Carlsbad, California) with a LED light source (CoolLED; Andover, United Kingdom) mounted on a SteREO Lumar microscope.v12 (Zeiss; Jena, Germany). Static images were obtained for each hindlimb every 8 seconds over a 30-min period. Using these images, lymphatic pumping in a

standardized region of interest over the dominant collecting lymphatic vessel was analyzed with Fiji software (NIH; Bethesda, MD). After subtracting the background fluorescent intensity, fluctuations in intensity within the lymphatic vessel were plotted over time, with each fluctuation corresponding to a lymphatic contraction. The initial 10 min of each image series were excluded to avoid inaccuracies from inadvertent lymphatic stimulation due to positioning. Lymphatic contractions per minute were quantified as packet frequency.[38]

Immune cell trafficking analysis

DC migration was assessed following PLND using a modification of previously reported methods.[39] Briefly, 20 μl of type I isomer FITC (diluted as 5 mg/ml; Sigma-Aldrich) was mixed 1:1 with acetone and dibutyl phthalate (Sigma-Aldrich) and circumferentially painted on the distal hindlimb footpad skin. After 18 hours, the mice were sacrificed, and the draining inguinal lymph nodes (the nodes just proximal to the excised popliteal lymph nodes) were collected for analysis. Single-cell suspensions were created by mechanically dissociating and enzymatically digesting the inguinal lymph nodes with a combination of DNase I, Dispase II, and collagenase D (Roche Diagnostics; Indianapolis, IN). Endogenous Fc receptors were blocked with rat monoclonal anti-CD16/CD32 (#14-0161-85; eBioscience; San Diego, CA), after which the cells were stained with Armenian hamster anti-CD11c antibodies (N18; #117309; BioLegend; San Diego, CA). Cells were also incubated with DAPI to allow for the exclusion of dead cells. Single-stain compensations were created using hindlimb tissue in which FITC was not injected and UltraComp eBeads™ (#01-2222-42, Affymetrix, Inc.; San Diego, CA). Flow cytometry was performed to identify $CD11c^{+}FITC^{+}$ DCs using a Fortessa flow cytometer (BD Biosciences; San Jose, CA) with BD FACS Diva. Data were analyzed with FlowJo software (Tree Star; Ashland, OR).

Statistical analysis

Data were analyzed and displayed using GraphPad Prism software version 9.2.0 (GraphPad Software; San Diego, CA). Differences between the two groups were assessed with the paired (clinical samples) and unpaired (mice samples) Student's t-test, while comparisons over time were conducted using a two-way analysis of variance with Tukey's multiple comparisons test. Normal distribution was assessed, and parametric or non-parametric tests were used when appropriate. Data are presented as mean ± standard deviations, and $P < 0.05$ was considered significant.

Results

Lymphedematous tissue has increased ACE and Ang II expression

Using matched tissue obtained from the lymphedematous and contralateral upper extremities from 8 patients with breast cancer-related lymphedema (BCRL) (Table 1), we analyzed the expression of ACE and Ang II protein (Figures 1a, b). Higher ACE expression was detected in the lymphedematous versus normal tissue in 7 out of 8 patients, with an average increase of 2.3-fold (Figure 1a, p=0.001). Although western blotting for Ang II was technically difficult, presumably due to lower tissue expression of the protein, we found higher Ang II expression in lymphedematous versus normal tissue in 5 of 8 patients evaluated, although this difference was not statistically significant overall (Figure

1a p=0.09). Using immunofluorescence (IF), we noted increased expression of ACE in the lymphedematous tissues compared with normal skin in 13 out of 14 patients, with an average increase of 2.4-fold (Figure 1b, p=0.0002). Higher Ang II expression was detected in the lymphedematous tissues of 11 out of 14 patients, with an average increase of 1.4-fold (Figure 1b, p=0.04). Analysis of gene expression (Figure 1c) also showed higher expression of angiotensinogen (2.9-fold, p=0.03), ACE (2.6-fold, p=0.01), and angiotensin II receptor type I (AT1R; 1.8-fold, p= 0.04) in lymphedematous versus normal tissue.

Topical captopril decreases lymphedema, fibrosis, and inflammation in a mouse tail model of lymphedema

We next tested the hypothesis that activation of the RAS in the skin plays a role in the pathophysiology of lymphedema using a mouse tail model of lymphedema. We developed a topical formulation of the ACE inhibitor captopril (5%) based on a case report using topical captopril to treat burn keloids in a single patient.[25] Two weeks after tail skin and lymphatic excision, mice were randomized to treatment with topical captopril or vehicle control (Aquaphor alone) once daily for 4 weeks. Treatment with topical captopril decreased tail swelling compared to control treatment, and these differences were statistically significant beginning 2 weeks after treatment (Figure 2a, b; p 0.001). By 6 weeks post-excision, captopril-treated mice had essentially no tail swelling; in contrast, control-treated mice still displayed significant tail edema. Comparing the area under the curve (AUC), there was a significant decrease (2.1-fold) in captopril-treated mice compared with controls (Figure 2c; p<.0001). These volumetric changes correlated with more edema and subcutaneous adipose tissue deposition in control mice (Figure 2d). Treatment with captopril resulted in 2.5-fold less fibroadipose tissue deposition compared with control treatment (Figure 2e; p=0.003).

Histological analysis showed that captopril treatment decreased ACE expression (Figure 3a; 1.7-fold, p=0.0006), the number of phosphorylated $Smad3^+$ cells ($pSmad3^+$; Figure 3b; 2.2 fold, p=0.008), and type I collagen deposition (Figure 3c; 1.7-fold, p=0.03) in the tail skin. The expression of pSmad3, a pivotal intracellular effector of TGF-β, decreased both in the epidermis and dermis. Lymphatic capillaries and collecting vessels in captopril-treated mice were markedly less dilated and had decreased surrounding collagen deposition compared with control-treated mice. In addition, treatment with captopril resulted in lymphangiogenesis and 2.3-fold more $LYVE\text{-}1^+$ lymphatic vessels that crossed the area of lymphatic ablation compared with control mice (Figure 3d; p=0.0005). These findings were supported by our Western blot studies demonstrating that captopril treatment increased VEGF-C protein in tail tissues (12.5-fold increase, p=0.0001; Supplementary figure 1).

Hyperkeratosis is a histological hallmark of lymphedema, and TGF-β activity regulates keratinocyte proliferation.[40] Consistent with this, we found that treatment with topical captopril decreased the number of proliferating keratinocytes (Figure 3e; 1.6-fold decrease, p=0.01) in the tail skin epidermis compared with control treatment.

The fibrotic process in lymphedema is closely tied to chronic inflammation resulting from lymphatic stasis. The inflammatory infiltrate is comprised of T cells and macrophages, which tend to cluster around lymphatic vessels.[3, 26, 27, 31, 41, 42] Consistent with

this, we found that treatment with topical captopril significantly decreased accumulation of perilymphatic $CD3^+$ T cells (1.9-fold) and $F4/80^+$ macrophages (1.4-fold) compared with control-treated mice (p=0.04) (Figure 4a, b).

Topical captopril improves lymphatic function after lymph node dissection

Mouse tail lymphatics have low-level pumping capacity making it difficult to assess changes in collecting lymphatic function after tail surgery.[43] In contrast, lymphatic collectors in the mouse hindlimb display strong contractions that can be quantified using ICG lymphography.[44, 45] Therefore, we used a mouse PLND model to assess the potential for topical captopril to improve lymphatic pumping.[28, 46, 47] Beginning two weeks after PLND, mice were treated with topical captopril or vehicle control ointment for 2 weeks. As expected, PLND did not result in significant tail swelling (not shown).[26, 48] Nevertheless, consistent with our findings using the tail model of lymphedema, we found that expression of ACE was significantly decreased in the dermis of captopril-treated compared with control-treated mice (Figure 5a; 1.6-fold, p=0.02). Similarly, captopril treatment resulted in lymphangiogenesis and higher numbers of $LYVE\text{-}1^+$ vessels (Figure 5b; 2.3-fold, p<0.0001). Lymphatic channels in captopril-treated mice were less dilated than in control-treated mice, suggesting improved outflow of interstitial fluid (Figure 5b, **far right**; 2.7-fold, p=0.01). High-power views of the collecting lymphatics in the distal hindlimb showed that lymphatic smooth muscle coverage was decreased in captopril-treated mice (Figure 5c; 1.5-fold, p=0.02).

Analysis of collecting lymphatic pumping function using Indocyanine Green (ICG)-lymphography showed that captopril treatment significantly increased the number of pumps/minute (i.e., packet frequency) following PLND (Figure 5d, e; 5-fold, p<0.0001). Consistent with improved lymphatic function, we also found that captopril treatment significantly increased trafficking of dermal dendritic cells to the inguinal lymph node (Figure 5f; 5-fold, p=0.002).

Discussion

In this study, we show that the expression of ACE is significantly increased in lymphedematous skin both in human clinical samples and mouse models of the disease. Inhibition of this response with topical captopril significantly decreased the pathology of lymphedema in mouse models by decreasing fibrosis, intracellular Smad3-phosphorylation, inflammation, and improving lymphatic function. These findings suggest that the RAS in the skin plays an important role in the regulation of fibrosis in lymphedema, and inhibition of this signaling pathway may hold merit for treating lymphedema.

Although there are no prior reports on the role of the RAS in primary or secondary lymphedema, previous studies have shown that this system, acting through Ang II, plays an important role in fibrosis in other organ systems by regulating extracellular matrix deposition, inflammation, and fibroblast proliferation.[14, 49–51] Once thought to act only systemically, locally acting, autologous RASs exist in almost all tissues of the body including the cardiovascular, renal and respiratpry systems, brain, liver, fat and skin.[52–54]

Our findings are also consistent with previous studies demonstrating an important role for the RAS in the regulation of hypertrophic scarring.[55–57] Finally, our finding that topical captopril decreases fibrosis in lymphedema aligns with studies demonstrating that blockade of the RAS attenuates architectural injury to inhibit fibrosis in the liver, colon, kidney, skin, and heart.[14, 25, 55, 56, 58–62]

Several lines of evidence suggest that Ang II regulates fibrosis by modulating intracellular TGF-β1 signaling or by promoting TGF-β1 production.[10, 15, 56, 63–72] AngII functions mainly through stimulation of two subtype receptors, angiotensin receptor 1 (AT1) and angiotensin receptor 2 (AT2).[73] While AngII induces fibrosis via the AT1 receptor, stimulation of the AT2 receptor may have regenerative effects and act to decrease fibrosis.[74] Binding of Ang II to the AT1 receptor activates the ERK/p38/MAPK pathway resulting in Smad2 and Smad3 phosphorylation. The activated Smad2 and Smad3 complex with Smad4 translocate into the nucleus leading to the transcription of TGF-β, procollagen I, procollagen III, and fibronectin. Direct activation of TGF-β and subsequent Smad signaling are also induced by AngII-AT1 binding.[75, 76] Ang II stimulation induces TGF-β1 mRNA and protein expression by cardiomyocytes and cardiac fibroblasts and treatment with ACE inhibitors decreases TGF-β1 levels in hypertrophied and infarcted myocardium.[64–69] Ang II-mediated TGF-β1 signaling plays an important role in pulmonary fibrosis and is thought to play a role in transition of normal lung fibroblasts to myofibroblasts in a TGF-β1 dependent manner.[70] The expression of AngII and TGF-β1 is also increased in fibrotic skin disorders including hypertrophic scars, keloids, and scleroderma.[56, 71, 72]

A recent study by our group demonstrated increased TGF-β1 and pSmad3 expression and signaling in breast cancer-related lymphedema samples. These finding were confirmed in immunohistochemistry, mRNA analysis and Western blotting.[10] Inhibition of TGF-β1 activity with neutralizing antibodies, dominant negative adenoviral vectors, or topical pirfenidone is effective for decreasing the pathology of lymphedema in the mouse tail model.[6, 9, 10, 29] These approaches, similar to our findings with captopril, decrease fibrosis and inflammation and increase lymphatic function. Importantly, long-term treatment with ACE inhibitors is well-tolerated [77] in contrast to long-term inhibition of TGF-β1 activity, which results in disturbances in immune responses, generation of autoreactive T cells, and autoimmune disorders.[78] Thus, inhibiting Ang II, leading to subsequent downstream profibrotic signaling pathways' inhibition may represent a novel and clinically translatable alternative.

We found that topical captopril markedly improved lymphatic pumping and transport of immune cells in mouse models of lymphedema. Treatment resulted in decreased accumulation of type I collagen fibers around capillary lymphatics and decreased accumulation of α-SMA$^+$ cells around collecting lymphatic vessels, suggesting that physical changes in the lymphatic network resulting from progressive fibrosis rather than direct injury to the lymphatic vasculature contribute to the lymphatic dysfunction of lymphedema. This finding is supported by clinical studies demonstrating progressive fibrosis of lymphatic collectors with worsening lower extremity lymphedema.[5] The important role of fibrosis in the pathophysiology of lymphedema is also supported by the finding that inhibition of radiation-induced fibrosis with small molecule inhibitors of TGF-β1 is more effective

than radioprotective measures designed to prevent direct radiation-induced injury to the lymphatic system.[79] Although the exact cellular mechanisms by which fibrosis decreases lymphatic function remain unknown, it is likely that these changes in the extracellular matrix disturb anchoring filament-mediated uptake of interstitial fluid by initial lymphatic vessels. Alternatively, increasing stiffness of the collecting or capillary lymphatic vessels may decrease the potential for propelling lymphatic fluid forward, as suggested by studies on isolated lymphatic vessels.[80–82] These interesting possibilities represent an attractive avenue for future research to better understand the pathophysiology of lymphedema.

TGF-β1 is not only a key regulator of fibrosis but is also an important immune modulator. The findings of our study support our previous studies, showing that increased TGF-β1 activity resulting from lymphatic injury also modulates T cell and macrophage inflammatory responses.[6, 10] Whether or not this outcome is due to a direct effect on inflammatory cells or reflective of the decreased interstitial fluid accumulation from improved lymphatic function remains unclear. However, our findings suggest that these responses are tightly linked, and we have previously shown that depletion of $CD4^+$ T cells significantly decreases tissue TGF-β1 expression.[6, 26, 27, 31] Ang II inhibition has a multitude of effects on many cell types and it is possible that the results we noted in our study were not entirely due to anti-inflammatory changes. For example, inhibition of ang II may have effects on blood flow or vascular permeability. However, an exhaustive analysis of vascular changes is beyond the scope of this study and less likely to show significant changes since our previous studies with anti-inflammatory treatments for lymphedema have shown no significant changes in vascular permeability.[83] Analyzing the other potential effects of AngII inhibition, however, may be important in future preclinical studies.

Previous studies have shown that ACE inhibition decreases tumor-induced lymphangiogenesis.[84, 85] In contrast, we found that that captopril treatment increased lymphangiogenesis and formation of collateral lymphatics in the mouse tail model of lymphedema and after popliteal lymphadectomy. This discrepancy may be related to our observation that captopril treatment increased VEGFC expression. In addition, it is also likely that the anti-inflamatory effects of captopril decrease the expression of anti-lymphangiogenic cytokines (e.g., TGF-β1, interferon gamma, interleukin 4, interleukin 13) after lymphatic injury.[86, 87] This hypothesis is supported by previous studies showing that lymphangiogenesis in lymphedema is regulated by a balance between lymphangiogenic and anti-lymphangiogenic cytokines.[86–88] In fact, it is important to note that the expression of VEGFC is *increased* in lymphedematous tissues and in the serum of patients with lymphedema suggesting that the pathophysiology of lymphedema is not due to a deficiency in lymphangiogenic cytokine expression.[88] Thus, even though ACE inhibition may have an anti-lymphangiogenic effects, these changes may be offset by decreased inflammation and decreased expression of anti-lymphangiogenic growth factors such as TGF-B1.[10, 26, 27, 31, 83, 89]

Conclusions

The skin RAS is activated in lymphedema, and local inhibition of this response with a topical ACE inhibitor is effective in preclinical mouse models of lymphedema. As

captopril is an FDA approved medication that has an established safety profile after oral administration, our current study sets the stage for future preclinical studies to evaluate systemic absorption, safety, efficacy and patient selectiom for this treatment for secondary lymphedema.

Supplementary Material

Refer to Web version on PubMed Central for supplementary material.

Acknowledgements

This research was supported in part by the NIH through R01 HL111130 awarded to B.J.M., T32 CA009501 (stipends for G.D.G.N, C.Ly, C.Li, J.G, G.H, A.C.), the Cancer Center Support Grant P30 CA008748, the Emerson Collective, and a Tri-Institutional Stem Cell Initiative grant. B.J.M is an advisor to PureTech Corp and the recipient of an investigator-initiated research award from Regeneron Corp; all other authors report no potential conflicts of interest. All authors have read the journal's authorship agreement and policy on disclosure of potential conflicts of interest.

REFERENCES

1. Rockson SG and Rivera KK, Estimating the population burden of lymphedema. Ann N Y Acad Sci, 2008. 1131: p. 147–54. [PubMed: 18519968]
2. Cormier JN, et al. , Lymphedema beyond breast cancer: a systematic review and meta-analysis of cancer-related secondary lymphedema. Cancer, 2010. 116(22): p. 5138–49. [PubMed: 20665892]
3. Dayan JH, et al. , Lymphedema: Pathogenesis and Novel Therapies. Annu Rev Med, 2018. 69: p. 263–276. [PubMed: 28877002]
4. Kataru RP, et al. , Fibrosis and secondary lymphedema: chicken or egg? Transl Res, 2019. 209: p. 68–76. [PubMed: 31022376]
5. Mihara M, et al. , Pathological steps of cancer-related lymphedema: histological changes in the collecting lymphatic vessels after lymphadenectomy. PLoS One, 2012. 7(7): p. e41126. [PubMed: 22911751]
6. Avraham T, et al. , Blockade of transforming growth factor-beta1 accelerates lymphatic regeneration during wound repair. Am J Pathol, 2010. 177(6): p. 3202–14. [PubMed: 21056998]
7. Blobe GC, Schiemann WP, and Lodish HF, Role of transforming growth factor beta in human disease. N Engl J Med, 2000. 342(18): p. 1350–8. [PubMed: 10793168]
8. Meng XM, Nikolic-Paterson DJ, and Lan HY, TGF-β: the master regulator of fibrosis. Nat Rev Nephrol, 2016. 12(6): p. 325–38. [PubMed: 27108839]
9. Sano M, et al. , Potential role of transforming growth factor-beta 1/Smad signaling in secondary lymphedema after cancer surgery. Cancer Sci, 2020. 111(7): p. 2620–2634. [PubMed: 32412154]
10. Baik JE, et al. , TGF-β1 mediates pathologic changes of secondary lymphedema by promoting fibrosis and inflammation. Clin Transl Med, 2022. 12(6): p. e758. [PubMed: 35652284]
11. Prud'homme GJ, Pathobiology of transforming growth factor beta in cancer, fibrosis and immunologic disease, and therapeutic considerations. Lab Invest, 2007. 87(11): p. 1077–91. [PubMed: 17724448]
12. Santos RAS, et al. , The renin-angiotensin system: going beyond the classical paradigms. Am J Physiol Heart Circ Physiol, 2019. 316(5): p. H958–h970. [PubMed: 30707614]
13. Morihara K, et al. , Cutaneous tissue angiotensin-converting enzyme may participate in pathologic scar formation in human skin. J Am Acad Dermatol, 2006. 54(2): p. 251–7.
14. Murphy AM, Wong AL, and Bezuhly M, Modulation of angiotensin II signaling in the prevention of fibrosis. Fibrogenesis Tissue Repair, 2015. 8: p. 7. [PubMed: 25949522]
15. Zhang Y, et al. , Telmisartan delays myocardial fibrosis in rats with hypertensive left ventricular hypertrophy by TGF-β1/Smad signal pathway. Hypertens Res, 2014. 37(1): p. 43–9. [PubMed: 24089264]

16. Jonsson JR, et al. , Angiotensin-converting enzyme inhibition attenuates the progression of rat hepatic fibrosis. Gastroenterology, 2001. 121(1): p. 148–55. [PubMed: 11438504]
17. Chen K, et al. , Inhibition of TGFbeta1 by anti-TGFbeta1 antibody or lisinopril reduces thyroid fibrosis in granulomatous experimental autoimmune thyroiditis. J Immunol, 2002. 169(11): p. 6530–8. [PubMed: 12444164]
18. Sun N, et al. , Angiotensin-Converting Enzyme Inhibitor (ACEI)-Mediated Amelioration in Renal Fibrosis Involves Suppression of Mast Cell Degranulation. Kidney Blood Press Res, 2016. 41(1): p. 108–18. [PubMed: 26881856]
19. Fang QQ, et al. , Angiotensin-converting enzyme inhibitor reduces scar formation by inhibiting both canonical and noncanonical TGF-β1 pathways. Sci Rep, 2018. 8(1): p. 3332. [PubMed: 29463869]
20. Töx U and Steffen HM, Impact of inhibitors of the Renin-Angiotensin-aldosterone system on liver fibrosis and portal hypertension. Curr Med Chem, 2006. 13(30): p.3649–61. [PubMed: 17168728]
21. Morrissey JJ, et al. , The effect of ACE inhibitors on the expression of matrix genes and the role of p53 and p21 (WAF1) in experimental renal fibrosis. Kidney Int Suppl, 1996. 54: p. S83–7. [PubMed: 8731201]
22. Wengrower D, et al. , Prevention of fibrosis in experimental colitis by captopril: the role of tgf-beta1. Inflamm Bowel Dis, 2004. 10(5): p. 536–45. [PubMed: 15472513]
23. Cohen EP, Fish BL, and Moulder JE, The renin-angiotensin system in experimental radiation nephropathy. J Lab Clin Med, 2002. 139(4): p. 251–7. [PubMed: 12024113]
24. Hye Khan MA, et al. , Epoxyeicosatrienoic acid analogue mitigates kidney injury in a rat model of radiation nephropathy. Clin Sci (Lond), 2016. 130(8): p. 587–99. [PubMed: 26772189]
25. Ardekani GS, et al. , Treatment of a Postburn Keloid Scar with Topical Captopril: Report of the First Case. Plastic and Reconstructive Surgery, 2009. 123(3): p. 112e–113e. [PubMed: 19116544]
26. Garcia Nores GD, et al. , CD4(+) T cells are activated in regional lymph nodes and migrate to skin to initiate lymphedema. Nat Commun, 2018. 9(1): p. 1970. [PubMed: 29773802]
27. Zampell JC, et al. , CD4(+) cells regulate fibrosis and lymphangiogenesis in response to lymphatic fluid stasis. PLoS One, 2012. 7(11): p. e49940. [PubMed: 23185491]
28. Hespe GE, et al. , Baseline Lymphatic Dysfunction Amplifies the Negative Effects of Lymphatic Injury. Plast Reconstr Surg, 2019. 143(1): p. 77e–87e.
29. Clavin NW, et al. , TGF-beta1 is a negative regulator of lymphatic regeneration during wound repair. Am J Physiol Heart Circ Physiol, 2008. 295(5): p. H2113–27. [PubMed: 18849330]
30. Rutkowski JM, et al. , Secondary lymphedema in the mouse tail: Lymphatic hyperplasia, VEGF-C upregulation, and the protective role of MMP-9. Microvasc Res, 2006. 72(3): p. 161–71. [PubMed: 16876204]
31. Avraham T, et al. , Th2 differentiation is necessary for soft tissue fibrosis and lymphatic dysfunction resulting from lymphedema. Faseb j, 2013. 27(3): p. 1114–26. [PubMed: 23193171]
32. Tian W, et al. , Leukotriene B(4) antagonism ameliorates experimental lymphedema. Sci Transl Med, 2017. 9(389).
33. Nakamura K, et al. , Anti-inflammatory pharmacotherapy with ketoprofen ameliorates experimental lymphatic vascular insufficiency in mice. PLoS One, 2009. 4(12): p. e8380. [PubMed: 20027220]
34. Gousopoulos E, et al. , Regulatory T cell transfer ameliorates lymphedema and promotes lymphatic vessel function. JCI Insight, 2016. 1(16): p. e89081. [PubMed: 27734032]
35. Tabibiazar R, et al. , Inflammatory manifestations of experimental lymphatic insufficiency. PLoS Med, 2006. 3(7): p. e254. [PubMed: 16834456]
36. Gousopoulos E, et al. , Prominent Lymphatic Vessel Hyperplasia with Progressive Dysfunction and Distinct Immune Cell Infiltration in Lymphedema. Am J Pathol, 2016. 186(8): p. 2193–2203. [PubMed: 27315777]
37. Ehrlich HP, et al. , Morphological and immunochemical differences between keloid and hypertrophic scar. Am J Pathol, 1994. 145(1): p. 105–13. [PubMed: 8030742]

38. Proulx ST, et al. , Use of a PEG-conjugated bright near-infrared dye for functional imaging of rerouting of tumor lymphatic drainage after sentinel lymph node metastasis. Biomaterials, 2013. 34(21): p. 5128–37. [PubMed: 23566803]
39. Wendland M, et al. , Lymph node T cell homeostasis relies on steady state homing of dendritic cells. Immunity, 2011. 35(6): p. 945–57. [PubMed: 22195748]
40. Domaszewska-Szostek A, Zaleska M, and Olszewski WL, Hyperkeratosis in human lower limb lymphedema: the effect of stagnant tissue fluid/lymph. J Eur Acad Dermatol Venereol, 2016. 30(6): p. 1002–8. [PubMed: 26869365]
41. Olszewski WL, The pathophysiology of lymphedema - 2012. Handchir Mikrochir Plast Chir, 2012. 44(6): p. 322–8. [PubMed: 23283812]
42. Ogata F, et al. , Excess Lymphangiogenesis Cooperatively Induced by Macrophages and CD4(+) T Cells Drives the Pathogenesis of Lymphedema. J Invest Dermatol, 2016. 136(3): p. 706–714. [PubMed: 27015456]
43. Razavi MS, et al. , Axial stretch regulates rat tail collecting lymphatic vessel contractions. Sci Rep, 2020. 10(1): p. 5918. [PubMed: 32246026]
44. Baish JW, Padera TP, and Munn LL, The effects of gravity and compression on interstitial fluid transport in the lower limb. Sci Rep, 2022. 12(1): p. 4890. [PubMed: 35318426]
45. Liao S, et al. , Impaired lymphatic contraction associated with immunosuppression. Proc Natl Acad Sci U S A, 2011. 108(46): p. 18784–9. [PubMed: 22065738]
46. Blum KS, et al. , Dynamics of lymphatic regeneration and flow patterns after lymph node dissection. Breast Cancer Res Treat, 2013. 139(1): p. 81–6. [PubMed: 23613202]
47. Kwon S, et al. , Spatio-temporal changes of lymphatic contractility and drainage patterns following lymphadenectomy in mice. PLoS One, 2014. 9(8): p. e106034. [PubMed: 25170770]
48. Ly CL, Kataru RP, and Mehrara BJ, Inflammatory Manifestations of Lymphedema. Int J Mol Sci, 2017. 18(1).
49. Xu J, et al. , Local angiotensin II aggravates cardiac remodeling in hypertension. Am J Physiol Heart Circ Physiol, 2010. 299(5): p. H1328–38. [PubMed: 20833959]
50. Gupta D, et al. , Renin angiotensin aldosterone system in pulmonary fibrosis: Pathogenesis to therapeutic possibilities. Pharmacol Res, 2021. 174: p. 105924. [PubMed: 34607005]
51. Sopel MJ, et al. , Myocardial fibrosis in response to Angiotensin II is preceded by the recruitment of mesenchymal progenitor cells. Lab Invest, 2011. 91(4): p. 565–78. [PubMed: 21116240]
52. Paul M, Poyan Mehr A, and Kreutz R, Physiology of local renin-angiotensin systems. Physiol Rev, 2006. 86(3): p. 747–803. [PubMed: 16816138]
53. Dzau VJ and Re R, Tissue angiotensin system in cardiovascular medicine. A paradigm shift? Circulation, 1994. 89(1): p. 493–8. [PubMed: 8281685]
54. Danser AH, et al. , Is there a local renin-angiotensin system in the heart? Cardiovasc Res, 1999. 44(2): p. 252–65. [PubMed: 10690302]
55. Stawski L, et al. , Angiotensin II induces skin fibrosis: a novel mouse model of dermal fibrosis. Arthritis Res Ther, 2012. 14(4): p. R194. [PubMed: 22913887]
56. Kawaguchi Y, et al. , Angiotensin II in the lesional skin of systemic sclerosis patients contributes to tissue fibrosis via angiotensin II type 1 receptors. Arthritis Rheum, 2004. 50(1): p. 216–26. [PubMed: 14730619]
57. Ardekani GS, et al. , Treatment of a postburn keloid scar with topical captopril: report of the first case. Plast Reconstr Surg, 2009. 123(3): p. 112e–113e. [PubMed: 19116544]
58. Cruz CI, et al. , Age-related progressive renal fibrosis in rats and its prevention with ACE inhibitors and taurine. Am J Physiol Renal Physiol, 2000. 278(1): p. F122–9. [PubMed: 10644663]
59. Osterreicher CH, et al. , Angiotensin-converting-enzyme 2 inhibits liver fibrosis in mice. Hepatology, 2009. 50(3): p. 929–38. [PubMed: 19650157]
60. Ambari AM, et al. , Angiotensin Converting Enzyme Inhibitors (ACEIs) Decrease the Progression of Cardiac Fibrosis in Rheumatic Heart Disease Through the Inhibition of IL-33/sST2. Front Cardiovasc Med, 2020. 7: p. 115. [PubMed: 32850979]

61. Koga H, et al. , Transanal delivery of angiotensin converting enzyme inhibitor prevents colonic fibrosis in a mouse colitis model: development of a unique mode of treatment. Surgery, 2008. 144(2): p. 259–68. [PubMed: 18656634]
62. Mezzano SA, Ruiz-Ortega M, and Egido J, Angiotensin II and renal fibrosis. Hypertension, 2001. 38(3 Pt 2): p. 635–8. [PubMed: 11566946]
63. Montezano AC, et al. , Nicotinamide adenine dinucleotide phosphate reduced oxidase 5 (Nox5) regulation by angiotensin II and endothelin-1 is mediated via calcium/calmodulin-dependent, rac-1-independent pathways in human endothelial cells. Circ Res, 2010. 106(8): p. 1363–73. [PubMed: 20339118]
64. Gray MO, et al. , Angiotensin II stimulates cardiac myocyte hypertrophy via paracrine release of TGF-beta 1 and endothelin-1 from fibroblasts. Cardiovasc Res, 1998. 40(2): p. 352–63. [PubMed: 9893729]
65. Campbell SE and Katwa LC, Angiotensin II stimulated expression of transforming growth factor-beta1 in cardiac fibroblasts and myofibroblasts. J Mol Cell Cardiol, 1997. 29(7): p. 1947–58. [PubMed: 9236148]
66. Kim S, et al. , Effects of an AT1 receptor antagonist, an ACE inhibitor and a calcium channel antagonist on cardiac gene expressions in hypertensive rats. Br J Pharmacol, 1996. 118(3): p. 549–56. [PubMed: 8762077]
67. Yu CM, et al. , Effects of combination of angiotensin-converting enzyme inhibitor and angiotensin receptor antagonist on inflammatory cellular infiltration and myocardial interstitial fibrosis after acute myocardial infarction. J Am Coll Cardiol, 2001. 38(4): p. 1207–15. [PubMed: 11583905]
68. Sun Y, et al. , Angiotensin II, transforming growth factor-beta1 and repair in the infarcted heart. J Mol Cell Cardiol, 1998. 30(8): p. 1559–69. [PubMed: 9737942]
69. Schultz Jel J, et al. , TGF-beta1 mediates the hypertrophic cardiomyocyte growth induced by angiotensin II. J Clin Invest, 2002. 109(6): p. 787–96. [PubMed: 11901187]
70. Abdul-Hafez A, Shu R, and Uhal BD, JunD and HIF-1alpha mediate transcriptional activation of angiotensinogen by TGF-beta1 in human lung fibroblasts. Faseb j, 2009. 23(6): p. 1655–62. [PubMed: 19211927]
71. Zhang K, et al. , Increased types I and III collagen and transforming growth factor-beta 1 mRNA and protein in hypertrophic burn scar. J Invest Dermatol, 1995. 104(5): p. 750–4. [PubMed: 7738352]
72. Tang HT, et al. , Angiotensin II induces type I collagen gene expression in human dermal fibroblasts through an AP-1/TGF-beta1-dependent pathway. Biochem Biophys Res Commun, 2009. 385(3): p. 418–23. [PubMed: 19465003]
73. Kaschina E and Unger T, Angiotensin AT1/AT2 receptors: regulation, signalling and function. Blood Press, 2003. 12(2): p. 70–88. [PubMed: 12797627]
74. de Gasparo M, et al. , International union of pharmacology. XXIII. The angiotensin II receptors. Pharmacol Rev, 2000. 52(3): p. 415–72. [PubMed: 10977869]
75. Wang W, et al. , Essential role of Smad3 in angiotensin II-induced vascular fibrosis. Circ Res, 2006. 98(8): p. 1032–9. [PubMed: 16556868]
76. Schiller M, Javelaud D, and Mauviel A, TGF-beta-induced SMAD signaling and gene regulation: consequences for extracellular matrix remodeling and wound healing. J Dermatol Sci, 2004. 35(2): p. 83–92. [PubMed: 15265520]
77. O'Keefe JH, et al. , Should an angiotensin-converting enzyme inhibitor be standard therapy for patients with atherosclerotic disease? J Am Coll Cardiol, 2001. 37(1): p. 1–8. [PubMed: 11153722]
78. Awad MR, et al. , Genotypic variation in the transforming growth factor-beta1 gene: association with transforming growth factor-beta1 production, fibrotic lung disease, and graft fibrosis after lung transplantation. Transplantation, 1998. 66(8): p. 1014–20. [PubMed: 9808485]
79. Xavier S, et al. , Amelioration of radiation-induced fibrosis: inhibition of transforming growth factor-beta signaling by halofuginone. J Biol Chem, 2004. 279(15): p. 15167–76. [PubMed: 14732719]

80. Scallan JP and Davis MJ, Genetic removal of basal nitric oxide enhances contractile activity in isolated murine collecting lymphatic vessels. J Physiol, 2013. 591(8): p. 2139–56. [PubMed: 23420659]

81. Gashev AA, et al. , Regional variations of contractile activity in isolated rat lymphatics. Microcirculation, 2004. 11(6): p. 477–92. [PubMed: 15371129]

82. Benoit JN, et al. , Characterization of intact mesenteric lymphatic pump and its responsiveness to acute edemagenic stress. Am J Physiol, 1989. 257(6 Pt 2): p. H2059–69. [PubMed: 2603989]

83. Gardenier JC, et al. , Topical tacrolimus for the treatment of secondary lymphedema. Nat Commun, 2017. 8: p. 14345. [PubMed: 28186091]

84. Lin QY, et al. , Angiotensin II Stimulates the Proliferation and Migration of Lymphatic Endothelial Cells Through Angiotensin Type 1 Receptors. Front Physiol, 2020. 11: p. 560170. [PubMed: 33013481]

85. Wang L, et al. , Effects of angiotensin-converting enzyme inhibitors and angiotensin II type 1 receptor blockers on lymphangiogenesis of gastric cancer in a nude mouse model. Chin Med J (Engl), 2008. 121(21): p. 2167–71. [PubMed: 19080179]

86. Zampell JC, et al. , Lymphatic function is regulated by a coordinated expression of lymphangiogenic and anti-lymphangiogenic cytokines. Am J Physiol Cell Physiol, 2012. 302(2): p. C392–404. [PubMed: 21940662]

87. Gousopoulos E, et al. , An Important Role of VEGF-C in Promoting Lymphedema Development. J Invest Dermatol, 2017. 137(9): p. 1995–2004. [PubMed: 28526302]

88. Jensen MR, et al. , Higher vascular endothelial growth factor-C concentration in plasma is associated with increased forearm capillary filtration capacity in breast cancer-related lymphedema. Physiol Rep, 2015. 3(6).

89. Oka M, et al. , Inhibition of endogenous TGF-beta signaling enhances lymphangiogenesis. Blood, 2008. 111(9): p. 4571–9. [PubMed: 18310502]

Brief Commentary

Background:

Transforming growth factor-beta 1 (TGF-β1)-mediated tissue fibrosis is an important regulator of lymphatic dysfunction in secondary lymphedema. However, TGF-β1 targeting can cause toxicity and autoimmune complications, limiting clinical utility. Angiotensin II (Ang II) modulates intracellular TGF-β1 signaling, and inhibition of Ang II production using angiotensin-converting enzyme (ACE) inhibitors, such as captopril, has antifibrotic efficacy in some pathological settings.

Translational Significance:

The angiotensin-renin system in the skin plays an important role in the regulation of fibrosis in lymphedema, and inhibition of this signaling pathway using toical ACE inhibition may hold merit for treating lymphedema in the clinical setting.

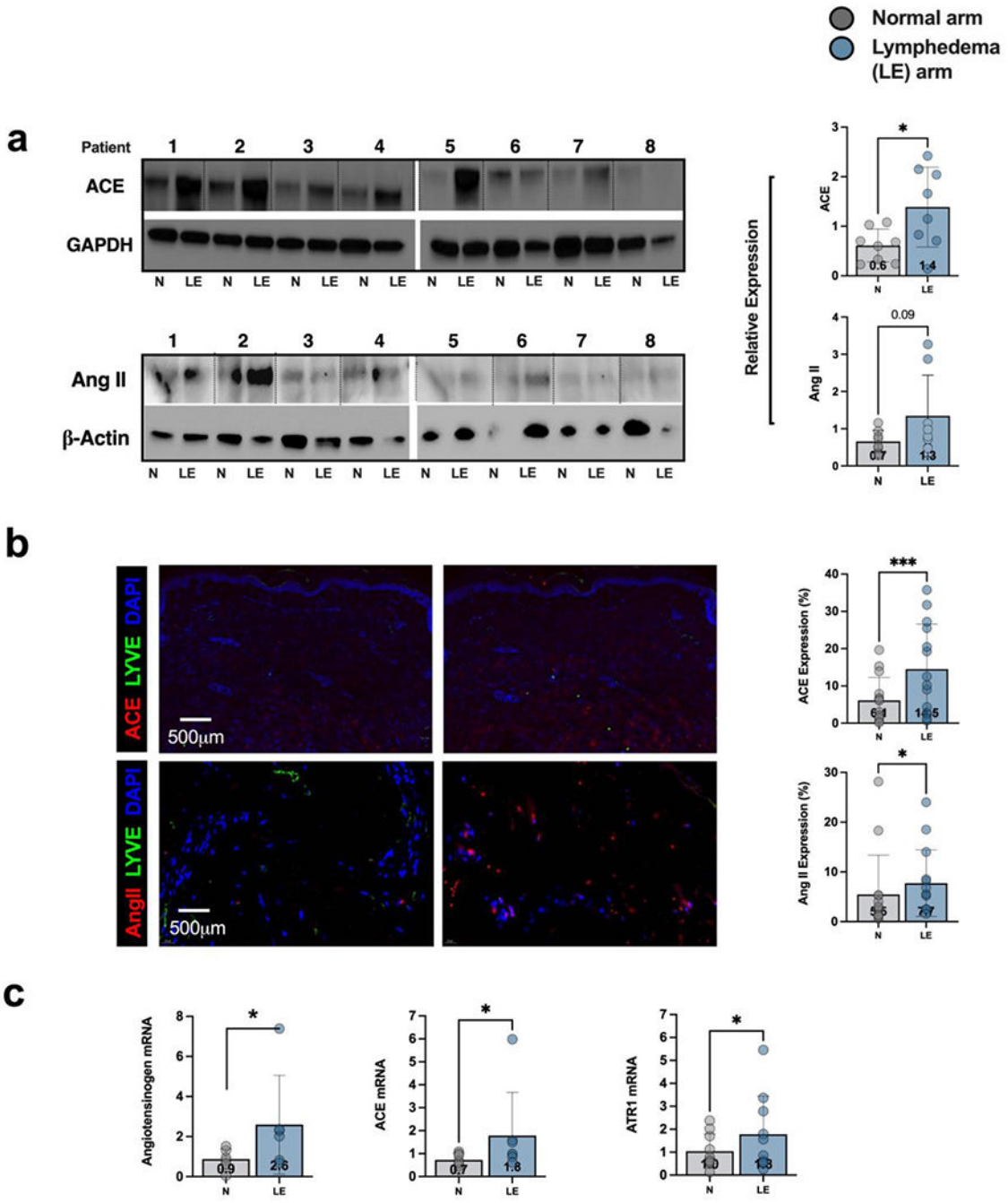

Figure 1. Expression of ACE is increased in clinical lymphedema skin biopsy samples.

a) Western blot analysis and quantification of ACE and Ang II expression in matched tissue obtained from the lymphedematous (LE) and contralateral normal (N) upper extremities of patients with breast cancer-related lymphedema (BCRL). Patient number is shown above each matched pair and separated by dotted lines. Each dot in the plots represents the average of two separate western blots. Data are mean ± standard deviation. Statistical analysis was performed using a matched t-test (*$p<0.05$).

b) Representative immunofluorescent images (left) and quantification (right) of ACE and Ang II in matched biopsies obtained from the lymphedematous (LE) and normal (N) upper extremities of patients with BRCL. Each dot in the graph represents the average of 2 high powered views (HPF; 40x) for each patient. Data are mean ± standard deviations. Statistical analysis was performed using a matched t-test (* $p<0.05$).

c) Gene expression of angiotensinogen, ACE, and angiotensin receptor I (AT1R) in matched biopsies obtained from the lymphedematous (LE) normal (N) upper extremities of patients with BRCL. Each dot in the graph represents the average of qPCR performed in triplicate for each patient and quantified using the delta delta method. Data are mean ± standard deviations. Statistical analysis was performed using a matched t-test on log normalized values (* $p<0.05$).

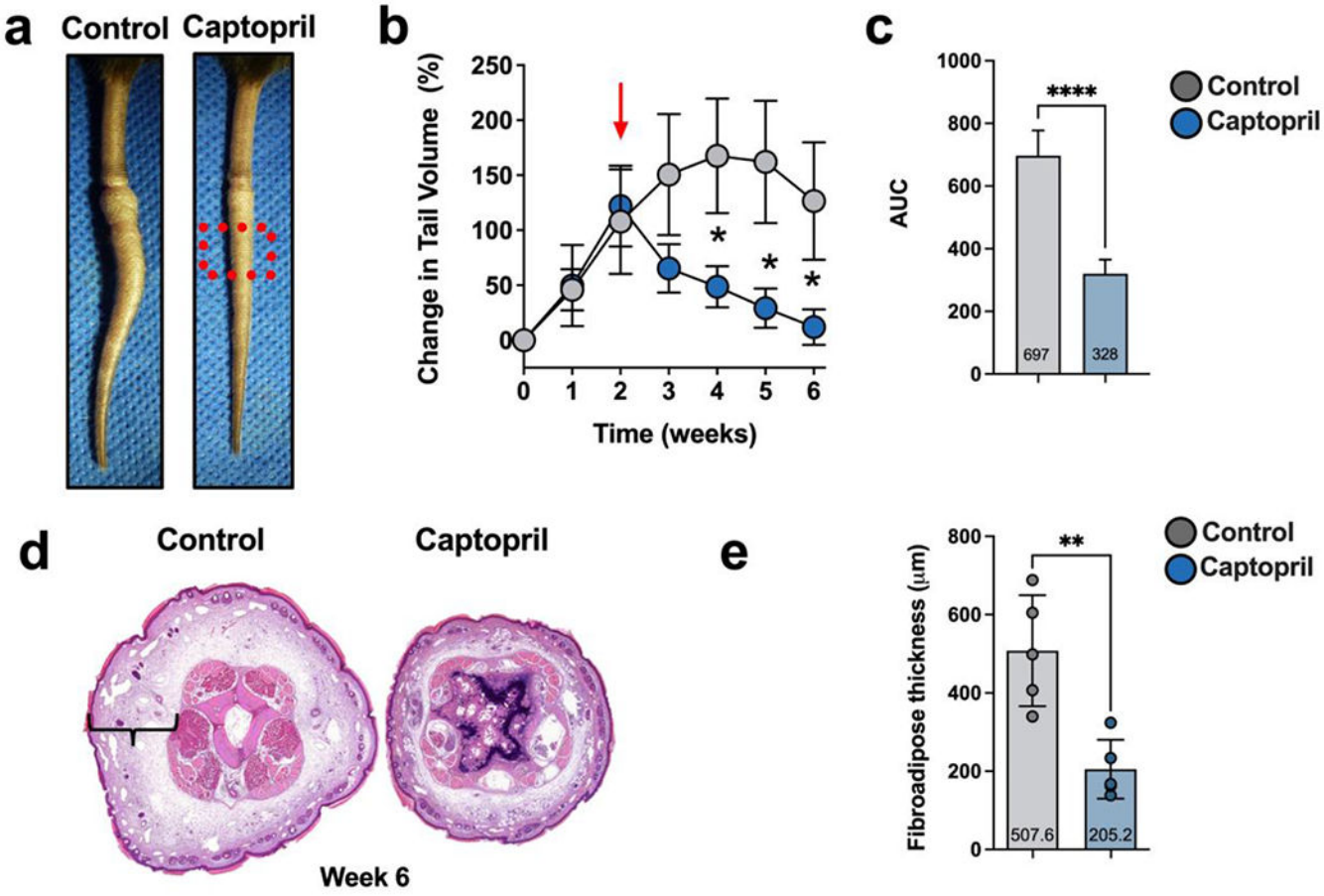

Figure 2. Topical captopril decreases edema and fibrosis in the mouse tail model of lymphedema 6 weeks after surgery.

a) Representative images of tail skin after treatment with control or topical captopril beginning 2 weeks after surgery. The red dotted box is the area analyzed using histology in H&E section shown in Figure 2d and Figures 3 and 4.

b) Quantification of tail volume changes using the truncated cone formula in mice treated with control or topical captopril. The red arrow indicates the time point when treatment was initiated. Statistical analysis was performed using a two-way ANOVA (* $p<0.05$).

c) Comparison of the area under the curve (AUC) in tail volume graph comparing captopril and control treated mice. Statistical analysis was performed using a t-test(**** $p<0.0001$).

d) Representative H&E staining of distal tail cross-sections in captopril and control treated mice. Brackets indicate fibroadipose thickness.

e) Quantification of tissue fibroadipose thickness in captopril and control treated mice. Each dot represents the average of 4 measurements for each mouse (n=7) used in the experiment. Data are mean ± standard deviation. Statistical analysis was performed using the Student's t test (**** $p<0.0001$).

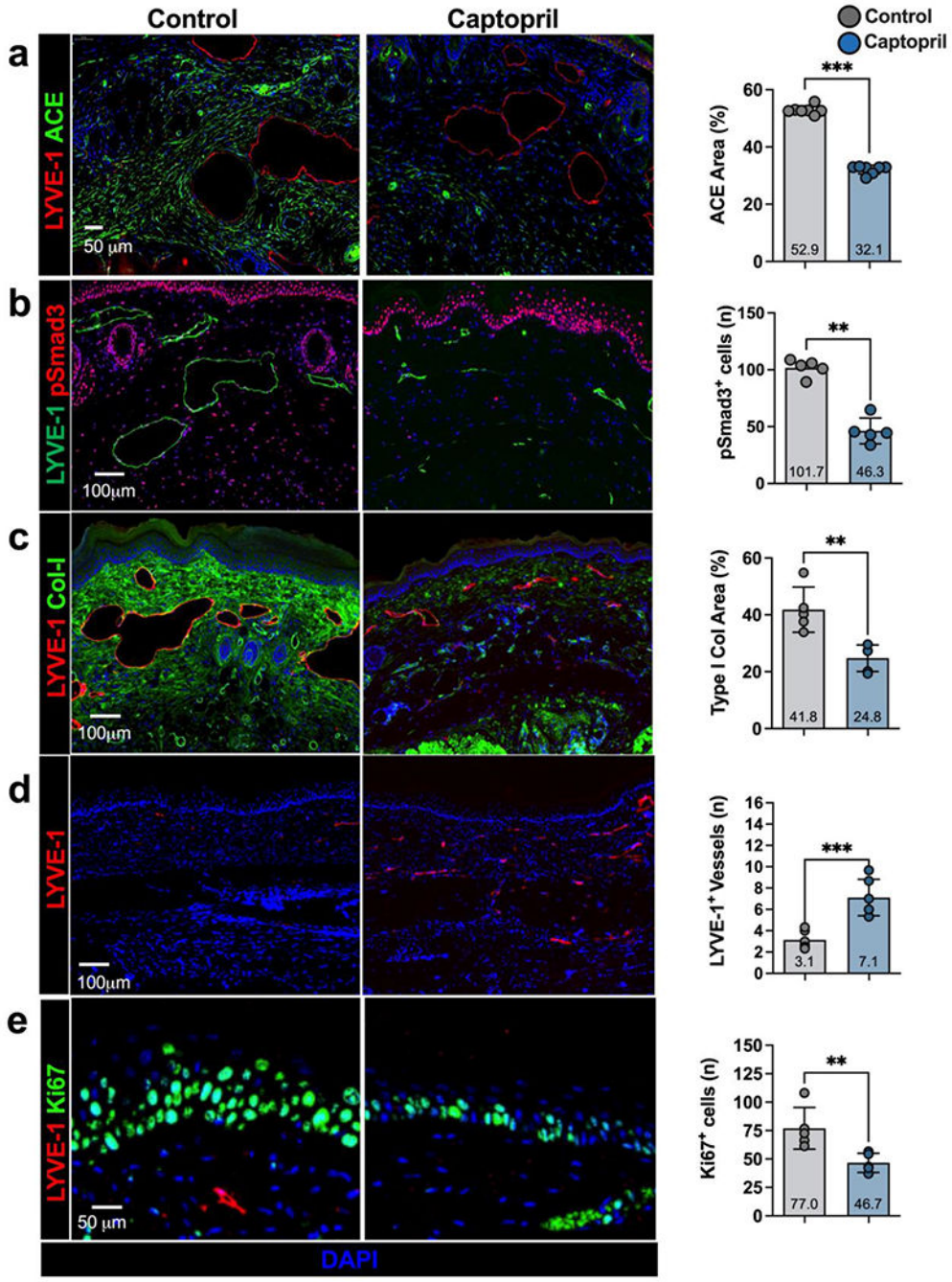

Figure 3. Topical captopril decreases ACE expression, SMAD phosphorylation, fibroadipose deposition, and hyperkeratosis in the mouse tail model of lymphedema.

a-e) Representative immunofluorescent images (left) and quantification (right) of ACE (a), pSmad3 (b), collagen I (Col-I; c), LYVE-1 (d), and Ki67 (e) in captopril and control treated mice 6 weeks after tail surgery. Each dot represents the average of 3 high powered views for each animal used in the analysis (n=7). Data are mean ± standard deviation. Statistical analysis was performed using the Student's t-test (*p<0.05, **p<0.01, ***p<0.001).

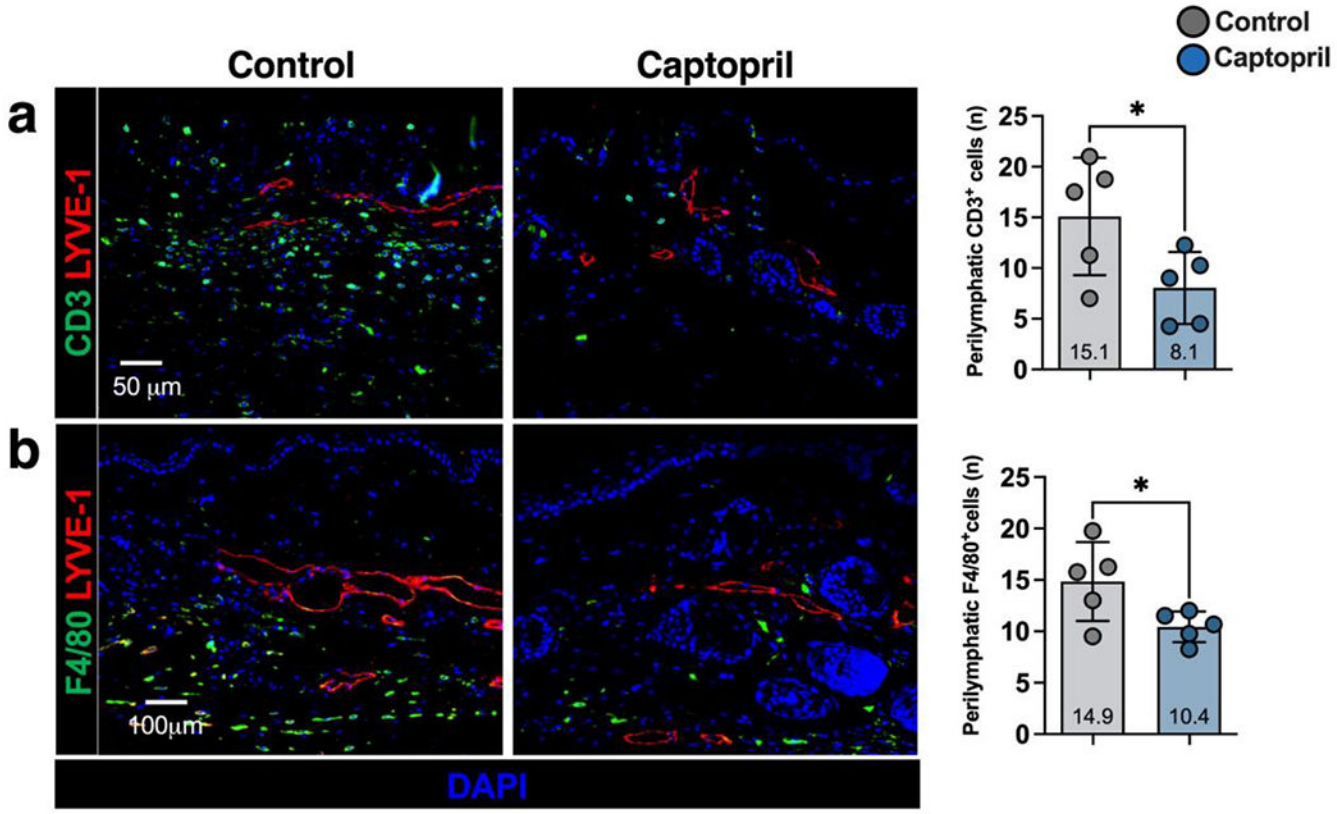

Figure 4. Topical captopril decreases inflammation in a mouse tail model of lymphedema.

a-b) Representative immunofluorescent images (left) and quantification (right) of LYVE-1 and $CD3^+$ (a) and $F4/80^+$ (b) cells in captopril and control treated mice 6 weeks after tail surgery. Each dot represents the average of 3 high powered fields for each animal (n=5) used in the analysis. Statistical analysis was performed using the Student's t-test (*$p<0.05$).

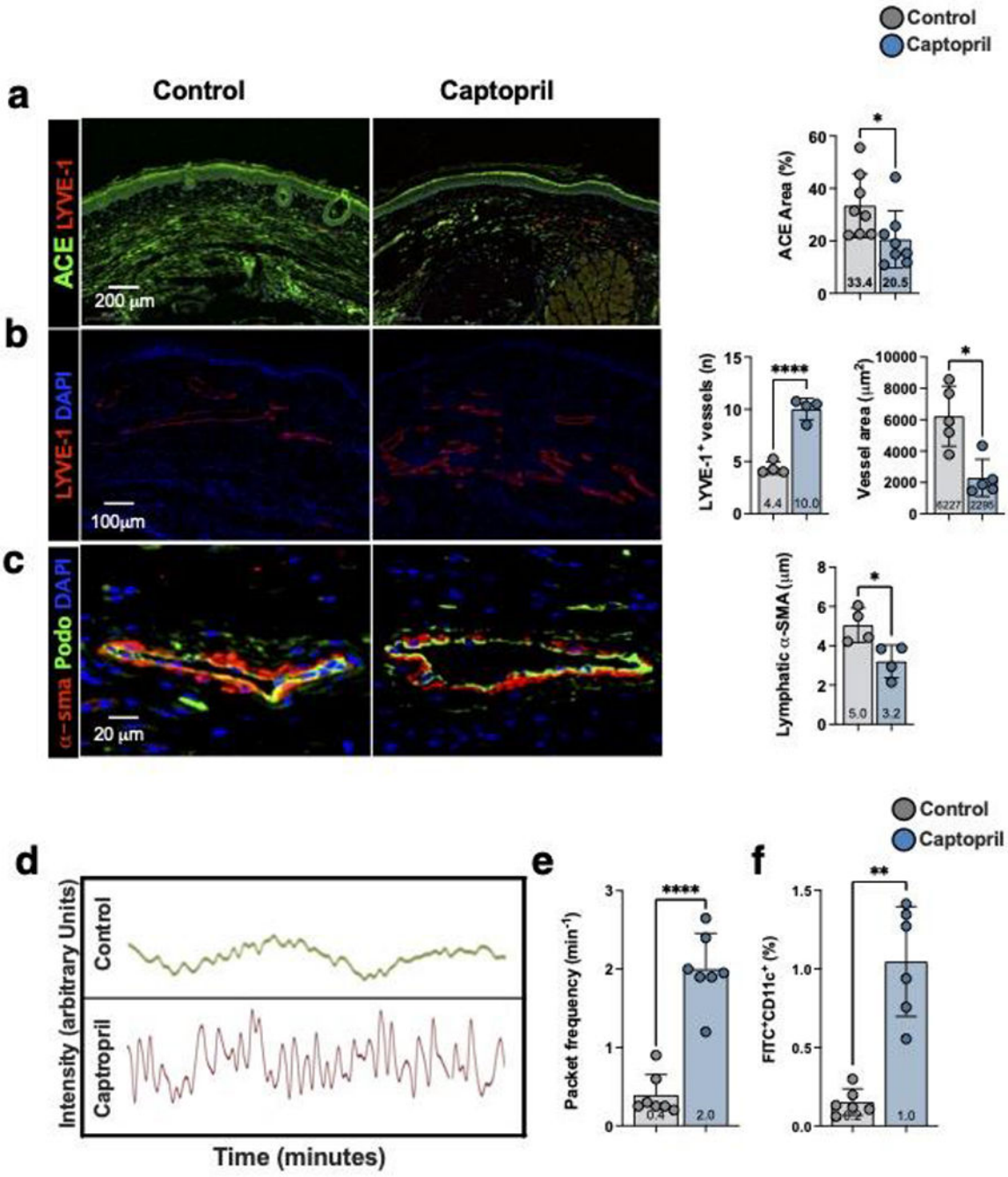

Figure 5. Topical captopril increases lymphangiogenesis and lymphatic function following PLND.

a) Representative immunofluorescent images (left) and quantification (right) of ACE in the skin of captopril or control treated mice 4 weeks after PLND. Each dot represents the average of 3 high power fields per animal (n=8) used in the study. Statistical analysis was performed using the Student's t-test (*$p<0.05$).

b) Representative immunofluorescent images (left) and quantification (right) localizing LYVE-1^+ lymphatic vessels in the skin of captopril or control treated mice 4-weeks after PLND. Quantification of LYVE-1^+ vessel diameter is also shown in the bar graphs on the

right. For the lymphatic vessel number, each dot represents the average number of lymphatic vessels in 3 low power fields (10x) per animal (n=4) used in the study. For the lymphatic vessel area, each dot represents the average of all vessels included in the images of 3 low power field per animal (n=5) used in the study. Statistical analysis was performed using the Student's t-test (*p<0.05, ****p<0.0001).

c) Representative immunofluorescent images localizing podoplanin (Podo) and α-SMA in collecting lymphatic vessels of captopril or control treated mice 4-weeks after PLND (left). Quantification of perilymphatic α-SMA thickness is shown to the right. Each dot represents the average thickness of α-SMA area in 4 quadrants of a collecting lymphatic for each animal (n=4) in the study. Statistical analysis was performed using the Student's t-test (*p<0.05).

d) Representative graphs depicting changes in near infrared fluorescence (NIR) in a collecting lymphatic vessel over time in captopril or control mice. Each peak represents a packet frequency.

e) Quantification of NIR collecting lymphatic vessel packet frequency in captopril and control treated mice. Each dot represents the average of 3 recordings in each mouse (n=7). Statistical analysis was performed using the Student's t-test (*p<0.0001).

f) Quantification of dendritic cell trafficking in captopril and control treated mice. FITC-acetone was painted on the distal hindlimb skin and the percentage of $FITC^{+}CD11c^{+}$ DCs in ipsilateral inguinal lymph nodes was quantified. Each dot represents the average of two flow-cytometry experiments for each mouse (n=6). Statistical analysis was performed using the Student's t-test (**p<0.01).

Table 1:

Demographic and Clinical Patient Information (clinical samples)

Patient	Age (years)	Gender	Body mass index (kg/m^2)	Volume Differential	LDEX score	History of hypertension	Hypertensive therapy history
1	62	Female	29.9	30.0	19	No	No
2	56	Female	23.7	32.3	47.8	No	No
3	43	Female	25.4	25.2	32	No	No
4	50	Female	28.9	79.6	89.6	No	No
5	56	Female	32.3	15.8	14.9	No	No
6	70	Female	29.69	142.2	429.6	No	No
7	56	Female	33.3	14.8	13.8	No	No
8	53	Female	24.6	63.3	70.3	No	No
9	52	Female	23.4	21.1	28	No	No
10	66	Female	26.9	3.4	10.2	No	No
11	51	Female	27.8	33.6	52.7	No	No
12	66	Female	29.2	34.7	74.4	No	No
13	51	Female	29.8	21.1	11.3	No	No
14	50	Female	26.5	25.9	27.3	No	No